### Stress-stress correlations reveal force chains in gels ®

Special Collection: Colloidal Gels

H. A. Vinutha @ ; Fabiola Doraly Diaz Ruiz @ ; Xiaoming Mao @ ; Bulbul Chakraborty @ ; Emanuela Del Gado  $extbf{ iny @}$ 



*J. Chem. Phys.* 158, 114104 (2023) https://doi.org/10.1063/5.0131473





CrossMark



The Journal of Chemical Physics

Special Topic: Adhesion and Friction

**Submit Today!** 





# 

Cite as: J. Chem. Phys. 158, 114104 (2023); doi: 10.1063/5.0131473

Submitted: 20 October 2022 • Accepted: 6 February 2023 •

Published Online: 15 March 2023







H. A. Vinutha,<sup>1</sup> Fabiola Doraly Diaz Ruiz,<sup>1</sup> Xiaoming Mao,<sup>2</sup> Bulbul Chakraborty,<sup>3</sup> and Emanuela Del Gado<sup>1,a)</sup> Substitution

#### **AFFILIATIONS**

- Department of Physics, Institute for Soft Matter Synthesis and Metrology, Georgetown University, Washington, DC 20057, USA
- <sup>2</sup>Department of Physics, University of Michigan, Ann Arbor, Michigan 48109, USA
- Martin Fisher School of Physics, Brandeis University, Waltham, Massachusetts 02453, USA

Note: This paper is part of the JCP Special Topic on Colloidal Gels.

a) Author to whom correspondence should be addressed: ed610@georgetown.edu

#### **ABSTRACT**

We investigate the spatial correlations of microscopic stresses in soft particulate gels using 2D and 3D numerical simulations. We use a recently developed theoretical framework predicting the analytical form of stress–stress correlations in amorphous assemblies of athermal grains that acquire rigidity under an external load. These correlations exhibit a pinch-point singularity in Fourier space. This leads to long-range correlations and strong anisotropy in real space, which are at the origin of force-chains in granular solids. Our analysis of the model particulate gels at low particle volume fractions demonstrates that stress–stress correlations in these soft materials have characteristics very similar to those in granular solids and can be used to identify force chains. We show that the stress–stress correlations can distinguish floppy from rigid gel networks and that the intensity patterns reflect changes in shear moduli and network topology, due to the emergence of rigid structures during solidification.

Published under an exclusive license by AIP Publishing. https://doi.org/10.1063/5.0131473

#### I. INTRODUCTION

Soft particulate gels consist of particulate matter (polymers, colloids, proteins, etc.) aggregated in a solid matrix, which is embedded in a fluid and typically sparse and porous. Gels of this type are found in the tissues of the body, food, drugs, personal care products, and even construction materials, such as the cement used in concrete. Their structures can be very soft and re-configurable, and their stress response is determined by a complex interplay between molecular cohesion or surface interactions, microstructural reorganization, and external driving. As a consequence, understanding, predicting, and designing the mechanics and rheology of these materials remains very challenging.

While particulate gels can be extremely soft because of the overall low solid content, the strength of the interactions that drive the aggregation of the colloidal units into the gel network must be large enough, with respect to  $k_BT$ , to overcome thermal fluctuations and stabilize the gel structural elements and their connections.<sup>4,5</sup> This implies that the elasticity is largely enthalpic in nature in these gels,

contrarily to polymer networks, and that the interaction strength, together with the total volume fraction of the solid content, controls elastic moduli, viscoelastic spectra, and nonlinear response. Remarkably, the interaction strength alone does not allow one to predict the gel properties. The morphology of the gel network, the structural elements, and their connectivity may change a lot due to different kinetics at play during the gel self-assembly, leading to huge variations of the mechanical response. This is sometimes the case even for identical compositions of the initial particle solution.

The solidification processes through which particulate gels form, initiated via, for example, irreversible fractal aggregation or equilibrium phase separation, are typically sources of frozenin stresses<sup>6</sup> and help build a memory in their history dependent response:<sup>7</sup> these processes determine how local stresses and mechanical heterogeneities get embedded and remain frozen inside the gel structure during gelation. The rigidity and elastic modulus attained ultimately depend on the geometry of the microstructure that self-assembles during solidification to accommodate the local and global constraints of mechanical equilibrium. Consequently, significant

structural correlations, induced, for example, by attractive interactions, are naturally incorporated in the way stresses are transmitted through the rigid backbone of the final solid. This process of self-organization can provide an explanation for the possible emergence of rigidity at very low densities in colloidal gels since the structural correlations developed are precisely those that satisfy the constraints of mechanical equilibrium, as shown in Ref. 8. The fact that this self-organization occurs in overall amorphous and spatially heterogeneous structures naturally leads to stress localization that manifests itself under deformation. 9–12

The tendency to localize strain and stresses and the signature of mechanical heterogeneities, shown under deformation, suggest that stress transmission could be very anisotropic and strongly localized even if the material is at rest, 13 just as a result of the microstructural development during gelation. As a consequence, force chains in a granular solid, i.e., forces transmitted across a sample along lines of grains forming a sparse network, <sup>14–18</sup> may be relevant to the physics of soft particulate gels. Detecting force chains and identifying the stress bearing part of gel structures are, however, incredibly difficult in experiments and elusive even in numerical simulations of model materials, as they require disentangling mechanical heterogeneities from structural heterogeneities and rely upon threshold values for local stresses that are not easily justified. For amorphous solids, recent theoretical studies have clarified that just the constraints of mechanical equilibrium guarantee that the spatial correlations of the stresses are long-ranged and anisotropic. 19-22 The emergence of elasticity can then be obtained, even in granular solids where the grain contacts cannot be regarded as elastic springs, within a new theoretical framework that can be mapped onto a tensorial electromagnetism with vector charges (VCT).<sup>23-25</sup> In particular, this VCT framework provides analytical predictions for the stress-stress correlations, demonstrating that they are not only long-ranged but also anisotropic, and clearly identifies the presence of force chains in disordered assemblies of grains that are jammed under an external load.

Here, we use the predictions of the VCT framework to compute the stress-stress correlations in model particulate gels obtained from 2D and 3D numerical simulations. We find that the intensity patterns of these correlations in Fourier and real space share several common features with the patterns detected in experiments and simulations of granular solids, as well as those predicted by the VCT framework. A particular, we recover the anisotropy of the stress-stress correlations, which therefore becomes an indicator of the presence of force chains in particulate gels. Moreover, we show that the stress-stress correlations distinguish floppy from rigid gels and are sensitive to the distance of the model gel from the rigidity threshold. These results pave the way to developing a further understanding of stress transmission in soft materials and provide the first basis to develop a VCT framework for soft gel materials.

This paper is organized as follows: Section II provides the details of the calculations performed: In Subsection II A, we briefly review the basic ingredients of the VCT framework and its predictions for the stress-stress correlations in granular solids, while Subsection II B contains information on the numerical models and simulations used. In Subsection II C, the calculations of the stress correlations are described. We then discuss the results in Sec. III and provide a summary and outlook in Sec. IV.

## II. THEORY PREDICTIONS AND NUMERICAL SIMULATIONS

## A. Elasticity theory of athermal amorphous solids and VCT framework

At the heart of the mechanical response of jammed amorphous solids is the nature of the force-bearing networks that obey the constraints of mechanical equilibrium. Implemented locally: each particle satisfies the constraints of force and torque balance. Here, bold symbols with hats denote tensors, bold symbols without hats denote vectors, and nonbold symbols denote components of tensors and vectors.

In a continuum formulation, the conditions of force balance expressed in terms of the stress tensor  $(\hat{\sigma})$  are given by

$$\partial_i \sigma_{ij} = f_j^{\text{ external}},$$
 (1)

where  $\sigma_{ij}$  is the stress component and  $f_j^{\text{external}}$  is the component of the external force. The torque balance leads to the symmetry of the stress tensor. However, in D dimensions, the conditions of mechanical equilibrium are not enough to solve for the D(D+1)/2 components of the stress tensor. Canonical continuum elasticity solves for the stress components by defining the strain in terms of the displacement field from the crystal reference structure, which is uniquely defined, and uses the constitutive relation of linear elasticity to obtain a complete set of equations.  $^{26,27,42}$  In the case of an amorphous solid, there is no unique reference structure to define the strain, so the continuum elasticity description does not work. The VCT framework described in Ref. 24 provides a stress-only framework to describe elasticity in such a solid. This stress-only theory of elasticity is defined by equations that bear a remarkable similarity to that of classical elasticity theory,  $^{25}$ 

$$\partial_{i}\sigma_{ij} = f_{j}^{\text{external}},$$

$$E_{ij} = \frac{1}{2} (\partial_{i}\varphi_{j} + \partial_{j}\varphi_{i}) \Longrightarrow \epsilon_{iab}\epsilon_{jcd}\partial_{a}\partial_{c}E_{bd} = 0,$$

$$\sigma_{ij} = (\delta_{ijkl} + \chi_{ijkl})E_{kl} \equiv K_{ijkl}E_{kl}.$$
(2)

Here,  $\hat{\sigma}$  is the stress–tensor field, which is related to  $\hat{E}$  via an emergent elastic modulus tensor  $\hat{K}$ .  $\hat{K}$  maps to the rank-4 polarizability tensor  $(\hat{\chi})$  of the VCT dielectric.  $\hat{E}$  plays a role analogous to the strain tensor in classical elasticity theory. External body forces, such as gravity, are represented by  $f^{\text{external}}$ . The two crucial differences from classical elasticity theory are that (a) the physical displacement field defining strain is replaced by the  $\varphi$  field, which is a gauge potential since there is no unique reference structure, and (b) the  $\hat{K}$  tensor is an emergent elastic modulus tensor that reflects the coarse-grained properties of the self-assembled, force-bearing network.

The VCT framework makes explicit predictions about the stress–stress correlations and the stress response in terms of the emergent elastic modulus tensor,  $\hat{\mathbf{K}}$ . Here, we summarize crucial features of the stress–stress correlations. (i) A hallmark of the theory is the appearance of a characteristic pinch-point in the stress–stress correlations,  $C_{ijkl}(\mathbf{q}) = \langle \sigma_{ij}(\mathbf{q})\sigma_{kl}(-\mathbf{q}) \rangle$ . A function of the wave vector  $|\mathbf{q}|$  has a pinch-point singularity in  $|\mathbf{q}| = 0$  if its value at  $\mathbf{q} = 0$  depends only on the orientation of any line passing through  $\mathbf{q} = 0$ . This means the dependence of the stress–stress correlations is

only on the angular coordinates in Fourier space for  $q \to 0$ . These predictions have been tested against experimental measurements in frictional granular materials and against model assemblies of frictionless soft grains in 2D and 3D. (ii) The chain-like structures seen, for example, in experiments using photoelastic discs<sup>24,28</sup> and commonly referred to as force-chains, are a visual representation of the highly anisotropic nature of  $C_{ijkl}$ . (iii) The q-space correlations predicted by the theory, and observed in experiments, imply a power-law decay at large lengthscales:  $\langle \sigma_{kl}(r)\sigma_{kl}(0)\rangle \propto \pm 1/r^D$ where the plus sign appears for longitudinal correlations and the minus sign for transverse correlations. In this paper, we analyze the stress-correlations in numerical simulations of 2D and 3D particle gels using the VCT framework.

#### **B. Simulation details**

Gel configurations in two and three dimensions are obtained using models of N interacting colloidal particles that undergo gelation as described in Refs. 8, 10, and 29-31. We perform Molecular Dynamics (MD) simulations in a cubic (square in 2D) box of size L with periodic boundary conditions. To prepare the gels, we first reach thermal equilibrium at a high temperature and then slowly quench the particle configurations to different target temperatures T, i.e., with different cooling rates  $C_r$ , using a Nosé-Hoover thermostat and allowing the particles to aggregate and form gel networks. <sup>29,32</sup> The mechanical equilibrium in the final gel states is obtained by slowly withdrawing all kinetic energies with overdamped dynamics, following the protocol described in Refs. 8, 10, and 31. All the simulations are performed using LAMMPS<sup>33</sup> modified by us to include specific particle interactions.

For 2D gels, we consider N = 10000 monodisperse particles interacting via a short range attractive potential  $U(r) = A\epsilon (a(d/r)^{18} - (d/r)^{16})$ , where r is the interparticle distance, and A and a are dimensionless constants. The values of A = 6.27 and a = 0.85 are chosen to obtain a short-ranged attractive well of depth  $\epsilon$  and range  $r_c \approx 0.3d$  (the potential is cut and shifted to 0 at large distances). In 3D, we consider  $N \approx 16\,000$  monodisperse particles that interact via the same short range attractive interactions plus an angular term that introduces bending rigidity to inter-particle bonds.

All the simulation quantities described in the following are expressed in reduced units; thus, d is used as the unit of length,  $\epsilon$ is used as the unit of energy, and m (the particle mass) is used as the unit of mass. The reduced temperature is expressed in units  $\epsilon/k_B$ , where  $k_B$  is the Boltzmann's constant. The unit of stress is therefore  $\epsilon/d^3$ . When performing the quenches into aggregation from a high temperature, the cooling rate  $C_r$  is defined as  $\Delta T/\Delta t$ , where  $\Delta T$  is the distance between the initial and target temperatures in the gelation protocol described earlier and  $\Delta t$  is the duration of the quench, with the unit time  $\tau_0$  being  $d\sqrt{m/\epsilon}$ . We define an approximate volume fraction  $\phi = \frac{\pi d^2 N}{4L^2}$  and  $\phi = \frac{\pi d^3 N}{6L^3}$  in two and three dimensions, respectively, where *d* is chosen as the particle diameter.

We consider that a gel configuration is rigid if the elastic component of the linear viscoelastic shear modulus at a low frequency is larger than the viscous component, which is true if there is a percolating rigid cluster. In 2D, we characterize such rigid gel configurations using the pebble game algorithm, which identifies a rigid cluster as a cluster where all the degrees of freedom are blocked

by contacts or constraints except for the degrees of freedom of the overall translations or rotations of the whole cluster. Therefore, in a rigid gel, there could be isolated particles or other small rigid clusters that are not part of the spanning cluster; however, the floppy modes associated with these isolated particles are not relevant to the low frequency elastic response of the sample. We call a gel floppy if in the particle configuration though there is a spanning network of aggregated particles, such network is not rigid according to the pebble game algorithm.<sup>8,34</sup> In 3D, we take another approach. We compute the linear viscoelastic response of the gels and obtain their low frequency moduli. <sup>29,30,35</sup> For rigid gels, the low frequency storage modulus is larger than the loss component.

In 2D, we show data for  $\phi = 0.5$  at T = 0.3 (floppy gels) and T = 0.18 (rigid gels). In 3D, we analyze gels obtained using the cooling rates  $C_r = 9 \times 10^{-5} \epsilon/(\tau_0 k_B)$ , and  $9 \times 10^{-2} \epsilon/(\tau_0 k_B)$  at  $\phi$  = 0.125, 0.075, and 0.05. All the data for the stress correlations have been averaged over 200 and 20 independently generated samples in 2D and 3D, respectively.

#### C. Computing stress correlation functions

To compute the stress correlations in the gel samples, we coarse-grain the stress fluctuations in Fourier space by imposing a cutoff at large q, corresponding to  $q_{\text{max}} = 2\pi/d$ , i.e., we do not consider any stress fluctuations occurring at length scales shorter than d. The lower q cutoff in Fourier space is set by the simulation box size  $q_{\rm min}$  =  $2\pi/L$  and the periodic boundary conditions. Following Refs. 24 and 25, for every particle p, we compute its contribution to the stress as the force-moment tensor defined as

$$\hat{\boldsymbol{\sigma}}_{\mathrm{p}} = \sum_{\mathrm{s}=1}^{N_{\epsilon}} \boldsymbol{r}_{\mathrm{p},\mathrm{s}} \otimes \boldsymbol{f}_{\mathrm{p},\mathrm{s}}, \tag{3}$$

where  $r_{p,s}$  is the vector connecting the center of particles p and s, and  $f_{p,s}$  is the force between them.  $N_c$  is the number of neighbors of particle p within the interaction range  $r_{p,s} \le r_c$ .

The force-moment tensor in Fourier space is given by

$$\hat{\boldsymbol{\sigma}}(\boldsymbol{q}) = \sum_{p=1}^{N} \hat{\boldsymbol{\sigma}}_{p} \exp(i\boldsymbol{q} \cdot \boldsymbol{r}_{p}), \tag{4}$$

where q stands for the wave vector and  $r_p$  is the p-th particle position vector. To obtain the stress tensor in Fourier space, we need to divide Eq. (4) by the volume (area) V of the simulation box; however, for simplicity, we ignore the constant factor of 1/V in our calculations. The stress correlations in Fourier space are computed using

$$C_{klmn}(\mathbf{q}) = \langle \Delta \sigma_{kl}(\mathbf{q}) \Delta \sigma_{mn}(-\mathbf{q}) \rangle, \tag{5}$$

$$\Delta \sigma_{kl}(\boldsymbol{q}) = \sum_{p=1}^{N} (\sigma_{klp} - \langle \sigma_{kl} \rangle) \exp(i\boldsymbol{q} \cdot \boldsymbol{r}_{p}), \tag{6}$$

where  $\sigma_{kl\,p}$  denotes kl-component of the stress tensor of particle p, and  $\Delta \sigma_{kl}$  represents the fluctuation of the stress tensor with respect to the average value  $\langle \sigma_{kl} \rangle$ . The angular brackets  $\langle \cdots \rangle$  denote an ensemble average, where each sample is first averaged over all the particles. For 3D gels, the computation of  $\hat{\sigma}_p$  also includes the contribution from the three body or angular term of the interaction potential.36

From the stress correlation calculations, we construct maps of the correlation intensity in Fourier space in polar  $(q,\theta)$  representation for 2D gels for a range of q from  $2\pi/L$  to  $56\pi/L$ . For the angular variation of the correlations, along with radial averaging, the data are also averaged over a small angular bin width of  $\approx 6^{\circ}$  to reduce noise. For comparison, we also compute the correlations in real space along both x and y direction with the coarse-graining length d.

In 3D, the range of q used is from  $2\pi/L$  to  $42\pi/L$ , the stress correlations are averaged over |q| and projected in 2D using the Hammer projection coordinate system  $(H_x, H_y)^{24,25}$   $H_x$  and  $H_y$  are computed using

$$H_x = \frac{2\sqrt{2}\cos\alpha\,\sin\beta/2}{\sqrt{1+\cos\alpha\,\cos\beta/2}},$$

$$H_y = \frac{\sqrt{2} \sin \alpha}{\sqrt{1 + \cos \alpha \cos \beta/2}},$$

where  $\alpha$  and  $\beta$  are the latitude and longitude, respectively.  $\alpha = \theta - \pi/2$  and  $\beta = \Phi$ , where  $(\theta, \Phi)$  are the spherical polar coordinate angles.

All stress correlations are scaled by the maximum value of the  $C_{xxxx}$  correlation function.

#### III. RESULTS

We now discuss the results obtained for 2D and 3D model particulate gels in mechanical equilibrium.

As discussed in the Introduction, soft particulate gels have strong structural heterogeneities that depend on the aggregation kinetics and the path to gelation. These structural heterogeneities are associated with stress heterogeneities; however, the microstructural origin of the stress heterogeneities is not easily identified. Figure 1 shows snapshots of a rigid gel close to the rigidity threshold8 (bottom panels) and a floppy gel (top panels) from our 2D simulations. The particles are colored according to their magnitude of xx and xy components of  $\hat{\sigma}_p$  computed using Eq. (3). The configurations in the top and bottom panels show connectivity percolation; however, the spanning rigid cluster, which was identified using the pebble game algorithm, is present only in the configuration of the bottom panel. In the floppy gel case, the particle stresses show strong, spatially uncorrelated fluctuations. In the rigid case, we observe that the particle stresses are spatially correlated and extended. For these numerical samples, these components of the stress tensor have a magnitude varying between  $-10\epsilon/d^3$  and  $8\epsilon/d^3$ . If we use the whole range for  $\sigma_{xx p}$  and  $\sigma_{xy p}$  in the color maps, the gels appear mechanically homogeneous, as they are overall soft. By zooming in the stress variation down to  $\Delta \sigma_{ij} \simeq 1\epsilon/d^3$ , chain-like patterns become visible in the stress maps of rigid gels. Floppy gels feature relatively large stress fluctuations even at this large stress magnification. These, however, appear randomly distributed and uncorrelated. For rigid gels, instead, the stress fluctuations display an anisotropic pattern, which strongly suggests an anisotropic and localized stress correlation across the sample and is reminiscent of force chains in granular packings. 14-18,28

These qualitative observations can be quantitatively confirmed by analyzing the intensity maps of the stress correlations for the

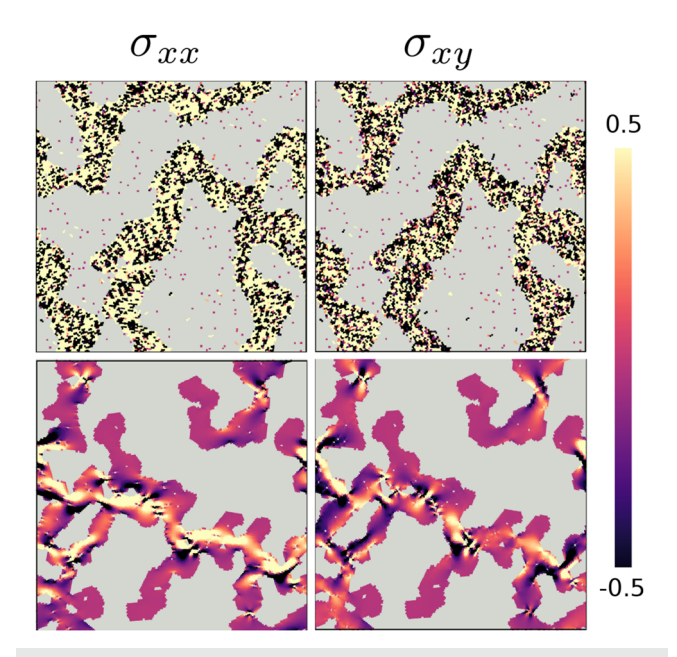


**FIG. 1.** Snapshots of 2D gel showing xx and xy components of the particle stresses for a floppy (top row) and rigid gel (bottom row).

corresponding component of the stress tensor, as shown in Fig. 2 (left). While for floppy gels the stress–stress correlation maps do not feature any distinctive pattern, for rigid gels they do. The patterns indicate both the presence of correlations that span the whole

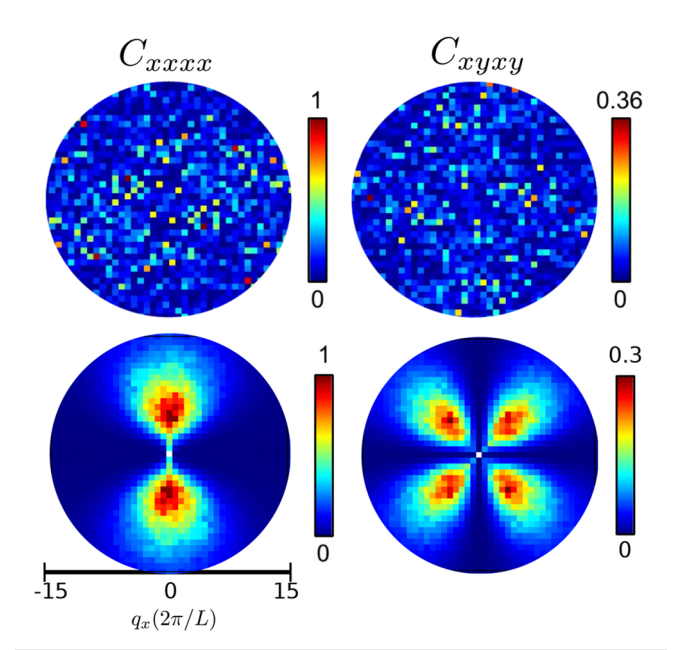


**FIG. 2.** Stress correlations  $C_{xxxx}$  and  $C_{xyxy}$  in Fourier space for the floppy and rigid gel in the top and bottom row, respectively.

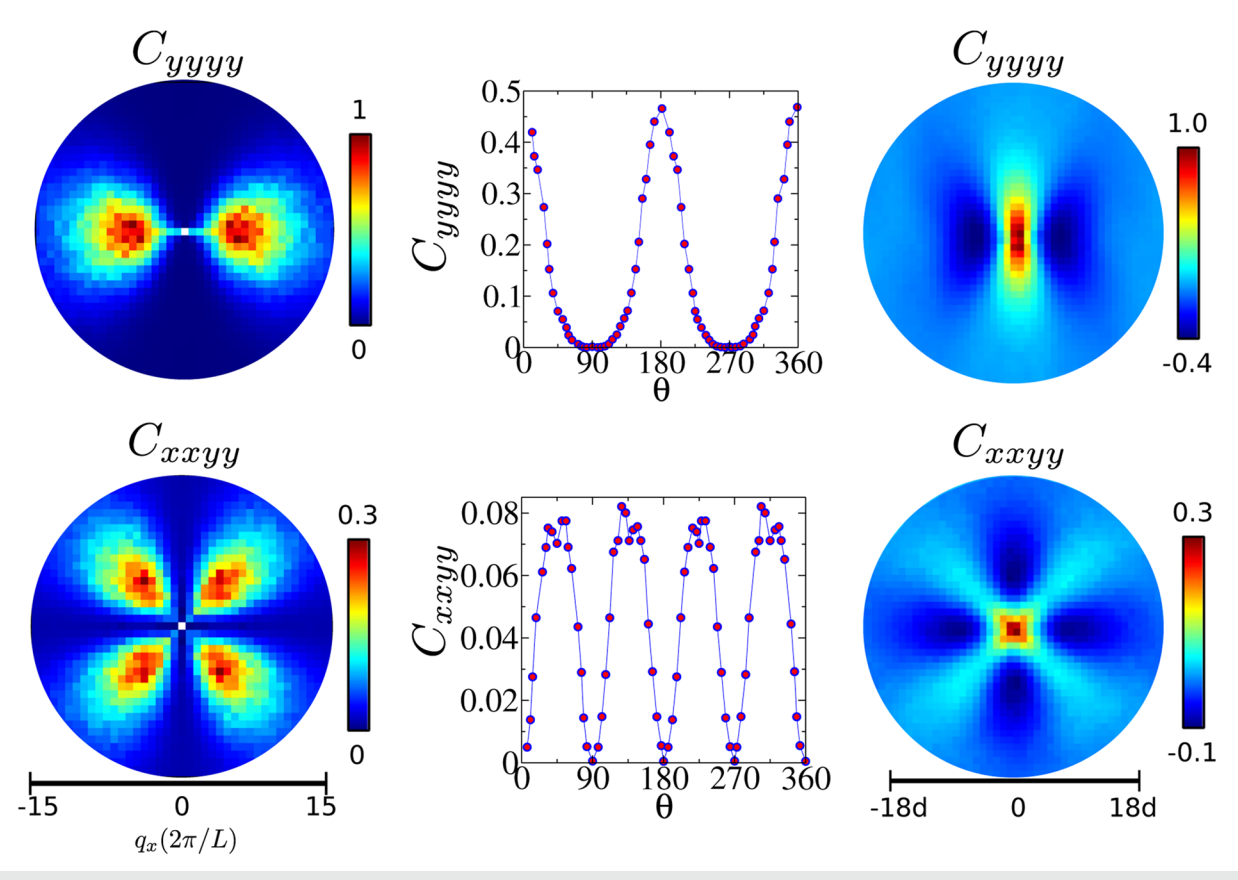


FIG. 3. Stress correlations  $C_{yyyy}$  (top row) and  $C_{xxyy}$  (bottom row) in q-space (left panel) and real space (right panel). In the middle panel, the angular dependence of the q-space correlations is shown.

system and that they do so in a very directional and anisotropic fashion, in spite of the particle interactions and the overall gels being isotropic. The  $C_{xxxx}$  map obtained from the rigid gels shows a large q cutoff in the correlations, which simply reflects the fact that well inside the gel branches the material is spatially and mechanically homogeneous. However, the correlation intensity is significant (along the  $q_x$  axis) even for the smallest  $q_x$ , i.e., for distances up to the whole system size. The value of  $C_{xxxx}$  being zero along the line  $q_v = 0$  indicates that the forces can propagate approximately only along their own direction and very unlikely perpendicular to it. At  $q \approx 0$ , the correlation intensity depends only on  $\theta$ , which is a signature of a pinch-point singularity. This is a direct consequence of force balance, as discussed in Sec. II A, and provides a quantitative evidence to the presence of force chains. The same characteristics, i.e., the long range correlations and the strong anisotropy indicated by the angular dependence, are also present in the four-lobe pattern of the  $C_{xyxy}$  map for the rigid gels (Fig. 2 right). We note that for  $C_{xyxy}$ the signal at low q is much weaker, since shear stresses are vanishing as there is no deformation applied.

The two-lobe pattern in  $C_{xxxx}$  and four-lobe pattern in  $C_{xyxy}$  for the rigid gels are identical to the correlation patterns already obtained in experiments and simulations of granular solids, confirming the pinch-point structure of stress

correlations in Fourier space predicted by the elasticity theory of the VCT framework.<sup>24</sup> In Fig. 3, we also show the  $C_{yyyy}$  (top) and  $C_{xxyy}$ (bottom) maps for the 2D rigid gels in Fourier space (left) and the corresponding radially averaged angular plots (center). The stress correlation maps in the real space (right) complement, and confirm, the insight gained with the maps of the correlations in Fourier space. The remaining stress correlations for 2D gels that consider all other stress tensor components are shown in Appendix A. These maps quantitatively establish the similarity of stress transmission in soft gels and in granular solids. They support the idea that the rigidity and elasticity of soft particulate gels, when particle interactions are sufficiently large with respect to  $k_BT$ , can be fundamentally understood as emerging properties that are the result of the local and global constraints imposed by mechanical equilibrium, rather than being just a consequence of their microscopic interactions. We note that, as briefly discussed in Sec. II A [see Eq. (2)], in the VCT framework, the angular dependence of the correlation intensity (Fig. 3 center) provides direct information on the properties of the emerging elastic tensor  $\hat{K}$ .

In the case of 3D gels, we have computed all 21 stress–stress correlations. We discuss some of them here in detail, while the remaining ones are shown in Appendix B. A snapshot of one of the gel networks [at volume fraction  $\phi = 0.125$  and obtained with

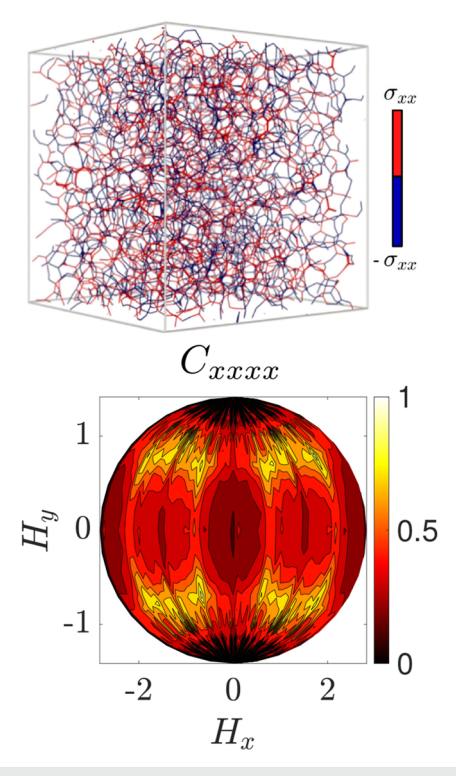


**FIG. 4.** (Top panel) Snapshot of the gel network at  $\phi = 0.125$ , only the bonds are shown. The particle bonds are red if the particle stress is positive and blue if the particle stress is negative. The bond width is proportional to the magnitude of the stress. (Bottom panel) Hammer projection of  $C_{xxxx}$  in Fourier space of the 3D gels at  $\phi = 0.125$ .

cooling rate  $C_r = 9 \times 10^{-5} \epsilon/(\tau_0 k_B)$ ] is shown in Fig. 4 (top panel). We have colored the particle bonds in red if the xx component of the particle stress is positive (tension) and blue if it is negative (compression) to highlight how, even with this information, the presence of force chains or stress localization cannot be easily detected. However, the maps of the corresponding stress correlation function clearly reveal their presence; furthermore, in this case, all stress–stress correlations are long-ranged, as determined by the mechanical equilibrium constraints; <sup>19,22</sup> the 2D Hammer projection of the correlation intensity for the fluctuations of the xx component of the stress tensor (Fig. 4, bottom panel) are strongly anisotropic, with the angular pattern indicating that stress transmit across the sample along specific and localized directions.

When comparing our data to the results in Ref. 24, we notice interesting quantitative differences in the corresponding angular plots. This suggests that the obvious significant differences between the overall elastic behavior of gels and granular solids can also be further investigated with this approach. In Fig. 5, we compare the intensity pattern of  $C_{zzzz}$  in rigid gels (top) and granular solids (bottom, from Ref. 25) to point out the striking difference in the angular dependence. As we increase the dimensionality of the space from 2D to 3D, the number of possible stress–stress correlation functions increases from 6 to 21, which provides more opportunity to identify the differences in the correlation patterns between the granular and gels case. We also note that our 3D gel model also features a

bending rigidity term in the particle–particle interactions, which is not present in the 2D case. This might also account for some additional differences in the intensity patterns between 2D and 3D, compared to the granular case. The map obtained for a model granular solid shows that the stress–stress correlations are basically independent on the azimuthal angle,  $\Phi$ , and only depend on  $\theta$ , whereas the pattern for the gels indicates a strong dependence on both  $\theta$  and  $\Phi$ , which confirms that this approach is able not just to reveal similarities and common traits but also to identify differences. With this respect, we think that this striking difference in the angular dependence may be related to the fact that all structures in a granular solid can only transmit compression or shear stresses, whereas in gels tension can also be transmitted. All the remaining stress correlations from 3D gels at  $\phi$  = 0.125 are shown in Appendix B.

The patterns of the stress correlations in gels are sensitive to the distance from the rigidity threshold, as shown by the  $C_{xzzz}$  maps in Fig. 6 at different  $\phi = 0.125, 0.075$  and 0.05 obtained for cooling rate  $C_r = 9 \times 10^{-5} \epsilon/(\tau_0 k_B)$ . As the volume fraction increases the local connectivity and gel moduli increase. At  $\phi = 0.05$ , the networks are sparse, spatially heterogeneous, and barely rigid, as also discussed in Refs. 30 and 37, and their elasticity modulus is very small. When particle volume fraction increases, the gels obtained with the same cooling rate become stiffer, more locally connected, and move away from the rigidity threshold. The stress correlations at different densities, interestingly, have the same general pattern. However, this pattern becomes increasingly blurred as the gels approach the rigidity threshold (Fig. 6 from left to right). A similar

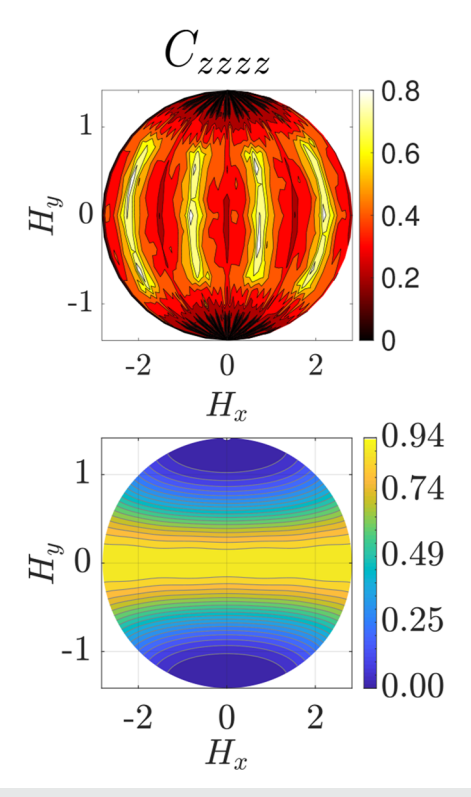


**FIG. 5.** Comparison of  $C_{zzzz}$  of gels at  $\phi=0.125$  (top figure) with the isotropic jammed solids (bottom figure). The jammed solids' data are from Ref. 25.

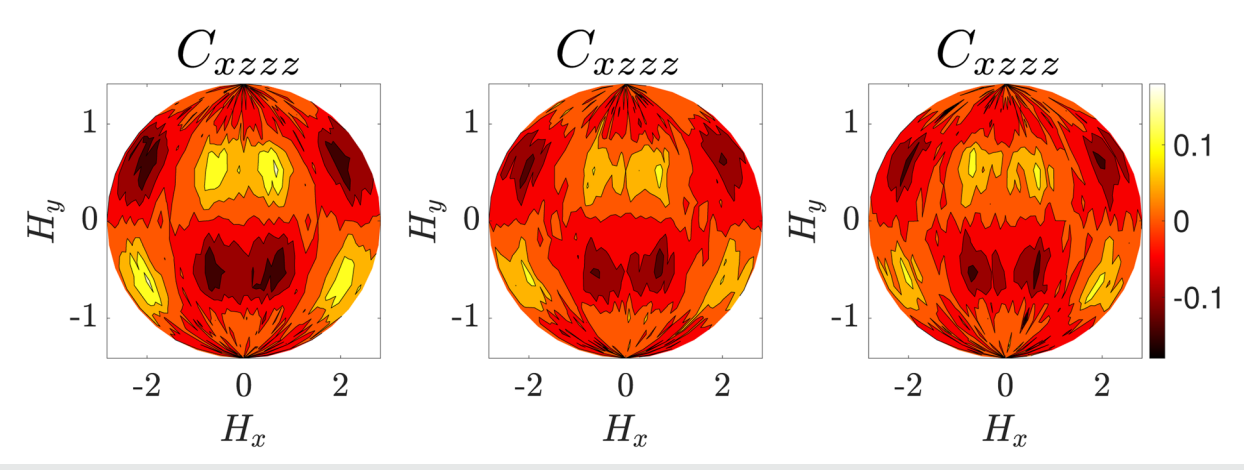


**FIG. 6.** Hammer projection of  $C_{xzzz}$  for the gel configurations at packing fraction 0.125 (left), 0.075 (middle) and 0.05 (right). The gel configurations are prepared with cooling rate  $C_r = 9 \times 10^{-5} \epsilon / (\tau_0 k_B)$ .

trend is observed in the correlations of all stress components. These findings support the idea that the stress correlation intensity variation is directly related to the elastic moduli, suggesting that they may be used to detect the distance from the rigidity threshold and provide information on the marginal stability of the gels. We also confirm these findings by varying, for the same particle volume fraction, the cooling rate at which the gel is formed, since the increasing this rate leads to gels that are weaker and closer to the rigidity threshold.<sup>37</sup> By comparing, for example, the stress correlation map in Fig. 7, which shows  $C_{xzzz}$  for  $\phi = 0.125$  at  $C_r = 9 \times 10^{-2} \epsilon/(\tau_0 k_B)$ , with the first map on the left of Fig. 6 [corresponding to the same volume fraction and  $C_r = 9 \times 10^{-5} \epsilon / (\tau_0 k_B)$ ], we can notice how again the correlation pattern becomes more blurred for weaker and more marginal gels. Clearly, the gels with the same density but different network elasticity result in changes in the stress-stress correlations. Since these are systems that are out of equilibrium, it is not obvious that there is a relation between the correlation function and the response function. Our results show that there could be such a relation. The VCT

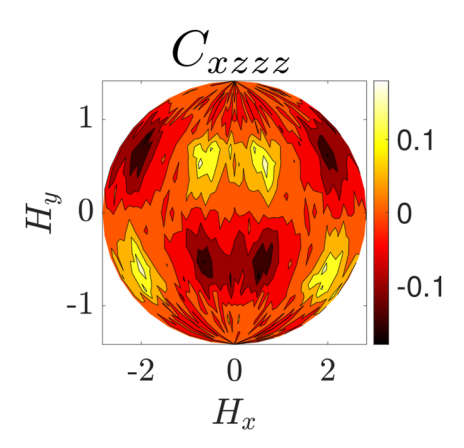


**FIG. 7.** Hammer projection of  $C_{xzzz}$  for the gel configurations at  $\phi=0.125$  and  $C_r=9\times 10^{-2}\epsilon/(\tau_0k_B)$ .

theory relates stress correlations to the elastic moduli with a one-to-one map between the full set of stress-correlations and the components of the  $\hat{K}$  tensor. <sup>24,25</sup>

#### **IV. SUMMARY**

In summary, we have demonstrated the presence of force chains in soft particulate gels by computing the stress-stress correlation functions in 2D and 3D model gels. The stress correlation patterns distinguish the rigid gels from the floppy gels and display the same general characteristics as granular solids, i.e., the strong angular dependence and the pinch point singularity predicted by a stress-only theoretical framework (the VCT framework in Ref. 24), where the elastic response is a property emerging only from the constraints of mechanical equilibrium without resorting to the constitutive relation of linear elasticity. We also demonstrate that the stress-stress correlation patterns highlight distinctive differences between gels and granular solids and that these patterns are sensitive to variation of the gel moduli due to changes in the gel topology and marginal stability, not simply to the gel density. These results are consistent with the idea that the stress-stress correlation patterns can provide further information on the tensorial properties of the emerging elasticity in these materials. Stress-stress correlation patterns have been measured in experiments on granular solids using photoelastic disks (see Ref. 24); however, this is clearly much more challenging for experiments on particulate gels, where measurement techniques to extract local stresses and their spatial distributions are still being developed.<sup>38–41</sup> Moreover, using the angular dependence of the stress-stress correlation functions obtained from simulations to extract the properties of the elastic tensor would provide predictions for the overall mechanical response to different deformation modes (e.g., shear, compression, and extension), which are accessible in mechanical and rheological experiments. This information, testable on a broad range of gels and experimental conditions, could then be fed back to the theory to obtain the stress-stress correlation patterns from the experiments. Hence, further developing the analysis proposed here seems a promising route to gain novel insight into

the emerging elasticity of soft particulate gels and its connection to stress localization.

#### **ACKNOWLEDGMENTS**

We thank Shang Zhang, Jishnu N. Nampoothiri, and Minaspi Bantawa for valuable discussions and configurations. This work was supported by the National Science Foundation (Grant Nos. NSF-DMR-2026842, NSF-DMR-2026825, and NSF-DMR-2026834) and the Clare Boothe Luce Program. Acknowledgment is made to the donors of the American Chemical Society Petroleum Research Fund for partial support of this research.

#### **AUTHOR DECLARATIONS**

#### **Conflict of Interest**

The authors have no conflicts to disclose.

#### **Author Contributions**

H. A. Vinutha: Conceptualization (lead); Data curation (lead); Formal analysis (lead); Writing – original draft (lead). Fabiola

Diaz Ruiz: Conceptualization (equal); Data curation (equal); Formal analysis (equal); Writing – original draft (equal). Xiaoming Mao: Conceptualization (equal); Data curation (equal); Investigation (equal); Methodology (equal); Supervision (equal); Writing – review & editing (equal). Bulbul Chakraborty: Conceptualization (equal); Data curation (equal); Investigation (equal); Methodology (equal); Supervision (equal); Writing – review & editing (equal). Emanuela Del Gado: Conceptualization (equal); Data curation (equal); Formal analysis (equal); Writing – original draft (equal).

#### DATA AVAILABILITY

The data that support the findings of this study are available within the article.

#### APPENDIX A: 2D CORRELATION FUNCTIONS

In Fig. 3, we show data for  $C_{yyyy}$  and  $C_{xxyy}$ . Here, we show all the remaining stress correlations for the rigid gels. The correlation functions are computed using Eq. (5). The angular dependence of these correlation functions matches with the granular case (Fig. 8).<sup>24</sup>

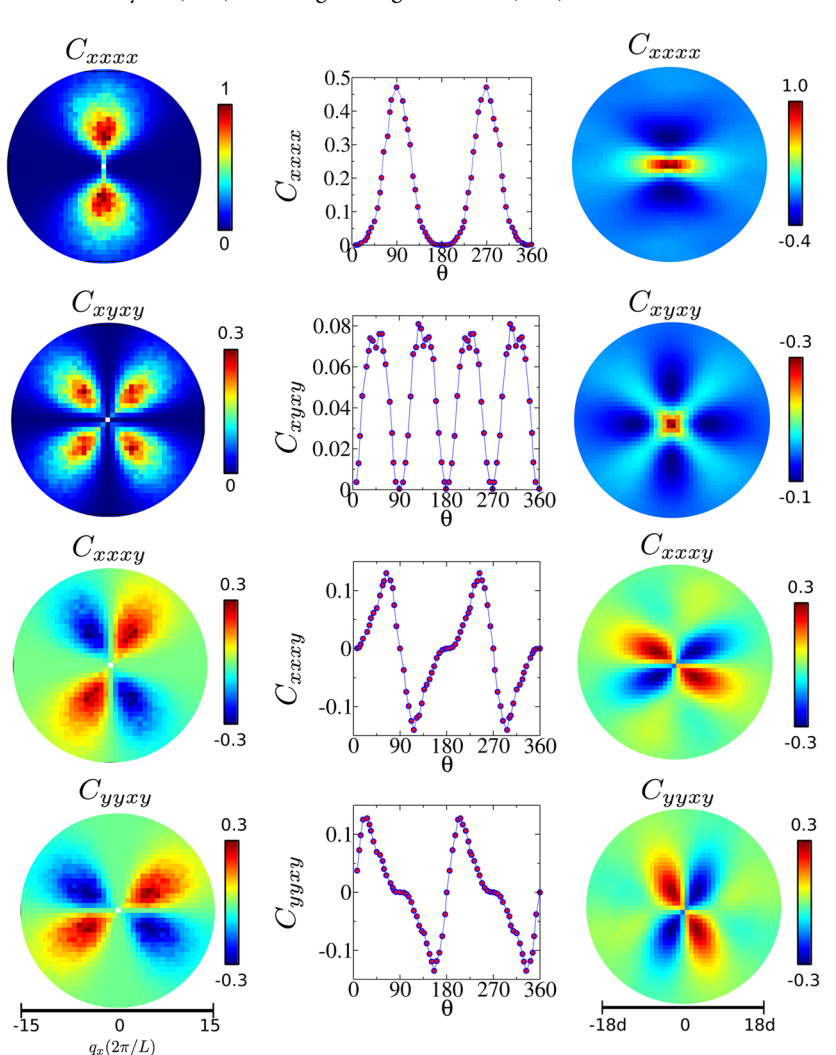


**FIG. 8.** The stress correlation functions for the 2D rigid gels. The three columns show the stress correlation in q-space, and the corresponding radially averaged angular plots and the stress correlation in real space, respectively.

#### APPENDIX B: STRESS CORRELATIONS IN FOURIER **SPACE FOR 3D GELS**

In this paper, we show  $C_{xxxx}$ ,  $C_{zzzz}$ , and  $C_{xzzz}$  correlation functions of gels at  $\phi$  = 0.125. In Fig. 9, the remaining 18 correlation functions are shown.

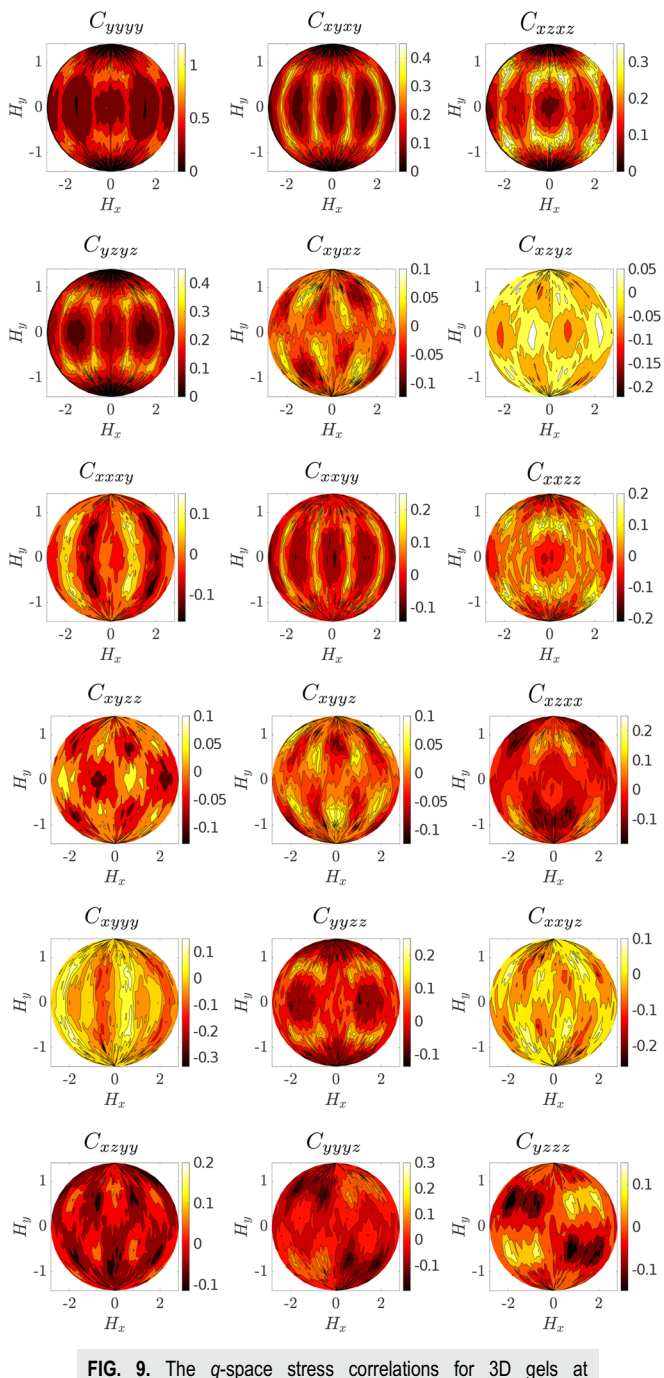


FIG. 9. The q-space stress correlations for 3D  $\phi = 0.125$ .

#### **REFERENCES**

- <sup>1</sup>E. D. Gado, D. Fiocco, G. Foffi, S. Manley, V. Trappe, and A. Zaccone, "Colloidal gelation," in Fluids, Colloids and Soft Materials (John Wiley & Sons, Ltd., 2016), Chap. 14, pp. 279-291.
- <sup>2</sup>G. Petekidis and N. J. Wagner, "Rheology of colloidal glasses and gels," in *Theory* and Applications of Colloidal Suspension Rheology (Cambridge University Press, 2021), pp. 173-226.
- <sup>3</sup>K. Ioannidou, M. Kanduč, L. Li, D. Frenkel, J. Dobnikar, and E. Del Gado, "The crucial effect of early-stage gelation on the mechanical properties of cement hydrates," Nat. Commun. 7, 12106 (2016).
- <sup>4</sup>V. J. Anderson and H. N. W. Lekkerkerker, "Insights into phase transition kinetics from colloid science," Nature 416, 811-815 (2002).
- <sup>5</sup>C. P. Royall, M. A. Faers, S. L. Fussell, and J. E. Hallett, "Real space analysis of colloidal gels: Triumphs, challenges and future directions," J. Phys.: Condens. Matter 33, 453002 (2021).
- <sup>6</sup>M. Bouzid, J. Colombo, L. V. Barbosa, and E. Del Gado, "Elastically driven intermittent microscopic dynamics in soft solids," Nat. Commun. 8, 15846 (2017).
- 7S. Zhang, E. Stanifer, V. Vasisht, L. Zhang, E. Del Gado, and X. Mao, "Prestressed elasticity of amorphous solids," Phys. Rev. Res. 4, 043181 (2021).
- <sup>8</sup>S. Zhang, L. Zhang, M. Bouzid, D. Z. Rocklin, E. Del Gado, and X. Mao, "Correlated rigidity percolation and colloidal gels," Phys. Rev. Lett. 123, 058001
- $^{\mathbf{9}}\text{M.}$  Leocmach, C. Perge, T. Divoux, and S. Manneville, "Creep and fracture of a protein gel under stress," Phys. Rev. Lett. 113, 038303 (2014).
- <sup>10</sup>J. Colombo and E. Del Gado, "Stress localization, stiffening, and yielding in a model colloidal gel," J. Rheol. 58, 1089-1116 (2014).
- <sup>11</sup>Z. Filiberti, R. Piazza, and S. Buzzaccaro, "Multiscale relaxation in aging colloidal gels: From localized plastic events to system-spanning quakes," Phys. Rev.  ${\rm E}$ 100, 042607 (2019).
- 12 S. Aime, L. Ramos, and L. Cipelletti, "Microscopic dynamics and failure precursors of a gel under mechanical load," Proc. Natl. Acad. Sci. U. S. A. 115, 3587-3592 (2018)
- 13 S. Alexander, "Amorphous solids: Their structure, lattice dynamics and elasticity," Phys. Rep. 296, 65-236 (1998).
- 14M. E. Cates, J. P. Wittmer, J.-P. Bouchaud, and P. Claudin, "Jamming, force chains, and fragile matter," Phys. Rev. Lett. 81, 1841 (1998).
- 15 F. Radjai, D. E. Wolf, M. Jean, and J.-J. Moreau, "Bimodal character of stress transmission in granular packings," Phys. Rev. Lett. 80, 61 (1998).
- <sup>16</sup>O. Gendelman, Y. G. Pollack, I. Procaccia, S. Sengupta, and J. Zylberg, "What determines the static force chains in stressed granular media?," Phys. Rev. Lett. 116, 078001 (2016).
- $^{\bf 17}{\rm H.~A.~Vinutha}$  and S. Sastry, "Force networks and jamming in shear-deformed sphere packings," Phys. Rev. E 99, 012123 (2019).
- 18 Y. Wang, Y. Wang, and J. Zhang, "Connecting shear localization with the longrange correlated polarized stress fields in granular materials," Nat. Commun. 11, 4349 (2020).
- <sup>19</sup>S. Henkes and B. Chakraborty, "Statistical mechanics framework for static
- granular matter," Phys. Rev. E **79**, 061301 (2009). <sup>20</sup>X. Mao, P. M. Goldbart, X. Xing, and A. Zippelius, "Soft random solids and their heterogeneous elasticity," Phys. Rev. E 80, 031140 (2009).
- <sup>21</sup>E. DeGiuli, "Field theory for amorphous solids," Phys. Rev. Lett. **121**, 118001
- <sup>22</sup> A. Lemaître, "Stress correlations in glasses," J. Chem. Phys. 149, 104107 (2018).  $^{\bf 23}{\rm M.}$  Pretko, "Generalized electromagnetism of subdimensional particles: A spin liquid story," Phys. Rev. B 96, 035119 (2017).
- <sup>24</sup>J. N. Nampoothiri, Y. Wang, K. Ramola, J. Zhang, S. Bhattacharjee, and B. Chakraborty, "Emergent elasticity in amorphous solids," Phys. Rev. Lett. 125,
- <sup>25</sup>J. N. Nampoothiri, M. D'Eon, K. Ramola, B. Chakraborty, and S. Bhattacharjee, "Tensor electromagnetism and emergent elasticity in jammed solids," Phys. Rev. E 106, 065004 (2022).
- <sup>26</sup>S. Timoshenko and J. N. Goodier, Theory of Elasticity: By S. Timoshenko and J. N. Goodier (McGraw-Hill, 1951).
- <sup>27</sup>L. Landau, L. Pitaevskii, A. Kosevich, and E. Lifshitz, *Theory of Elasticity* (Elsevier Science, 2012), Vol. 7.

- <sup>28</sup>R. P. Behringer and B. Chakraborty, "The physics of jamming for granular materials: A review," Rep. Prog. Phys. 82, 012601 (2018).
- <sup>29</sup>J. Colombo and E. Del Gado, "Self-assembly and cooperative dynamics of a model colloidal gel network," Soft Matter 10, 4003-4015 (2014).
- <sup>30</sup>M. Bouzid and E. Del Gado, "Network topology in soft gels: Hardening and softening materials," Langmuir 34, 773-781 (2018).
- <sup>31</sup>M. Bantawa, W. A. Fontaine-Seiler, P. D. Olmsted, and E. Del Gado, "Microscopic interactions and emerging elasticity in model soft particulate gels," J. Phys.: Condens. Matter 33, 414001 (2021).
- <sup>32</sup>M. G. Noro and D. Frenkel, "Extended corresponding-states behavior for particles with variable range attractions," J. Chem. Phys. 113, 2941-2944 (2000).
- 33S. Plimpton, "Fast parallel algorithms for short-range molecular dynamics," J. Comput. Phys. 117, 1-19 (1995).
- <sup>34</sup>D. J. Jacobs and B. Hendrickson, "An algorithm for two-dimensional rigidity
- percolation: The pebble game," J. Comput. Phys. 137, 346–365 (1997).

  35 M. Bouzid, B. Keshavarz, M. Geri, T. Divoux, E. Del Gado, and G. H. McKinley, "Computing the linear viscoelastic properties of soft gels using an optimally windowed chirp protocol," J. Rheol. 62, 1037-1050 (2018).

- <sup>36</sup>A. P. Thompson, S. J. Plimpton, and W. Mattson, "General formulation of pressure and stress tensor for arbitrary many-body interaction potentials under periodic boundary conditions," J. Chem. Phys. 131, 154107 (2009).
- <sup>37</sup>M. Bantawa, B. Keshavarz, M. Geri, M. Bouzid, T. Divoux, G. H. McKinley, and E. Del Gado, "The hidden hierarchical nature of soft particulate gels," arXiv:2211.03693 (2022).
- 38 R. C. Arevalo, P. Kumar, J. S. Urbach, and D. L. Blair, "Stress heterogeneities in sheared type-I collagen networks revealed by boundary stress microscopy," PLoS One 10, e0118021 (2015).
- $^{\bf 39}{\rm N.~Y.~C.}$  Lin and I. Cohen, "Relating microstructure and particle-level stress in colloidal crystals under increased confinement," Soft Matter 12, 9058-9067
- $^{\bf 40}{\rm A.}$  Gauthier, M. Pruvost, O. Gamache, and A. Colin, "A new pressure sensor array for normal stress measurement in complex fluids," J. Rheol. 65, 583-594 (2021).
- <sup>41</sup> J. Dong, F. Turci, R. L. Jack, M. A. Faers, and C. P. Royall, "Direct imaging of contacts and forces in colloidal gels," J. Chem. Phys. 156, 214907 (2022).
- 42 P. M. Chaikin, T. C. Lubensky, and T. A. Witten, Principles of Condensed Matter Physics (Cambridge University Press, Cambridge, 1995), Vol. 10.